Chapter 34
Characterization of Submarine Landslide Complexes Offshore Costa Rica: An Evolutionary Model Related to Seamount Subduction

Rieka Harders, César R. Ranero, and Wilhelm Weinrebe

Abstract Offshore Costa Rica large seamounts under-thrust the continental convergent margin causing slides of complex morphology. The large dimension of the structures has attracted previous investigations and their basic characteristics are known. However, no detailed mapping of their complex morphology has been reported. Here we present a detailed mapping of the failure-related structures and deposits. We use deep-towed sidescan sonar data, aided by multibeam bathymetry to analyze their geometry, geomorphologic character, backscatter intensity, and spatial distribution. Those observations are used to analyze the relationship between landslide characteristics and abundance, to the changes in the style of deformation caused by the subduction of seamounts to progressively greater depth under the margin.

Keywords Seamount subduction • Landslides • Deformation • Convergent margin • Model

34.1 Introduction

Underwater mass wasting processes occur at slopes of continental margins, flanks of volcanoes and large lakes. In this work we concentrate on submarine landsliding at the active subduction zone of the Middle America Trench (MAT) where the

R. Harders (✉) • W. Weinrebe
Geomar, Helmholtz-Zentrum für Ozeanforschung Kiel, Kiel, Germany
e-mail: riekaharders@gmx.de

C.R. Ranero
Barcelona Center for Subsurface Imaging (Barcelona-CSI), ICM, ICREA at CSIC, Barcelona, Spain

S. Krastel et al. (eds.), *Submarine Mass Movements and Their Consequences*, Advances in Natural and Technological Hazards Research 37, DOI 10.1007/978-3-319-00972-8_34,

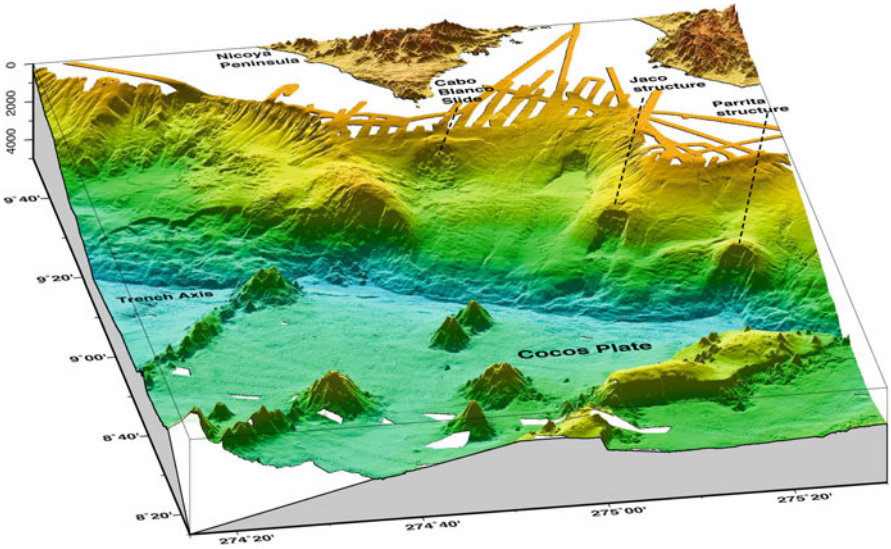

Fig. 34.1 Multibeam bathymetric map of the Middle America Trench offshore Costa Rica showing large-scale deformation and mass wasting structures in the margin related to seamount subduction

oceanic Cocos plate under-thrusts the Caribbean plate. Subduction zones can be differentiated between those with large accretionary prisms and those dominated by tectonic erosion, as the MAT, where tectonic processes gradually thin the overriding plate.

The convergent margin of the MAT has been extensively surveyed during the past two decades. Previous studies along >1,000 km of the MAT have shown that there exist more than 100 landslides with variable characteristics and origin. Work along the continental slope from Guatemala to Costa Rica identified submarine slides ranging in width and length from a few hundred meters to tens of km (Harders et al. 2011). The MAT slope displays evidence of mass-wasting structures with a distribution in segments, which appears similar to the segmentation of the morphology of the Cocos plate (Harders et al. 2011, 2012). Most large slides along the MAT occur where large seamounts subduct (Fig. 34.1). The seamounts are ~2–4 km high, ~20–30 km wide at their base, and cover ~40 % of the ocean plate offshore Costa Rica (Werner et al. 1999; von Huene et al. 2004).

Previous studies of slope failure at the MAT have been largely based on bathymetry data gridded at 100 m, with sufficient spatial resolution to detect large failure-related structures but not enough to map their internal structures and related deposits (Fig. 34.1). Sidescan sonar data have been locally used to complement those studies to classify large-scale failure structures (Hühnerbach et al. 2005; Ranero et al. 2008; Harders et al. 2011). However, the available sidescan sonar data permit detection of structures with a spatial resolution similar to a 25 m grid of high-quality multibeam bathymetry data (Kluesner et al. 2013). Thus, the

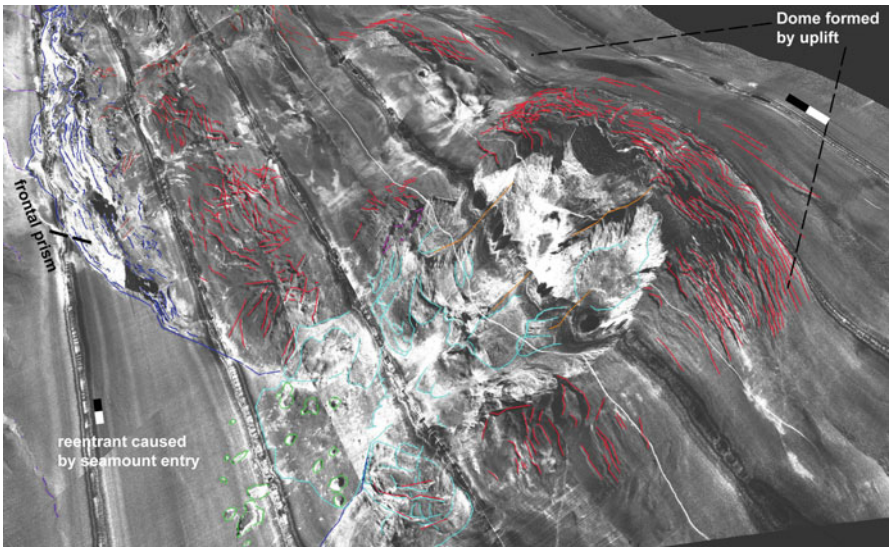

Fig. 34.2 Sidescan sonar imagery of Parrita structure. It shows a reentrant caused by seamount collision of Stage 1, a failed slope and associated structures, and the dome and deformation above an under-thrusting seamount of Stage 2. *Dark blue lines* are faults of the frontal prism. *Red lines* are fractures in slope sediment and possibly underlying margin wedge. *Pale blue* delineate debris flows. *Green polygons* delineate boulders from rock avalanches. *Orange lines* mark the crest of ridges. The *black-white bar* is 2 km long

sidescan sonar data allow for an improved analysis over previous work. Here we use sidescan sonar imagery draped on bathymetry for detailed mapping of Parrita and Jaco structures, and Cabo Blanco slide complex (Fig. 34.1). We differentiate deformational and mass-wasting related features based on morphology, geometry, and backscatter character (Figs. 34.2, 34.3, and 34.4). We use the three characteristic structures to propose a model of slope failure related to different stages of seamount under-thrusting that develop during the evolution in the subduction process.

34.2 Geological Framework

The bulk of the MAT overriding plate is made of competent crystalline rock, the so-called margin wedge, formed dominantly by igneous rock of the Caribbean flood basalt province and indurated sediment. The margin wedge is covered by ~0.5–2 km of slope sediment that is typically involved in landsliding. The front of the convergent margin is made of a 1–10 km wide sediment prism (Ranero and von Huene 2000; von Huene et al. 2000; Ranero et al. 2008). The frontal prism is formed by thrust sheets striking parallel to the trench, and is usually characterized by high backscatter caused by the rough relief produced by active faulting (Fig. 34.2).

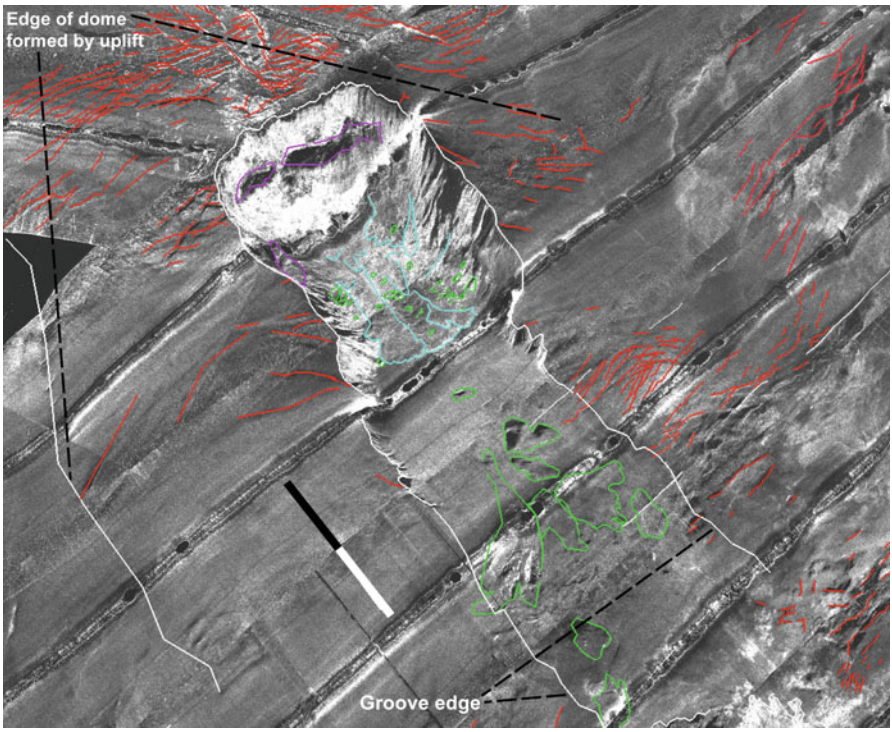

Fig. 34.3 Sidescan sonar imagery of Jaco structure. The dome, associated deformation, and the linear groove trailing the subducting seamount and mass-wasting structures define Stage 3. *Lilac polygons* delineate the *top* of blocks sliding on headwall and sidewall. *Red lines* mark fractures in slope sediment and possibly underlying margin wedge. *Pale blue* delineate debris flows. *Green polygons* delineate boulders from rock avalanches. The *black-white bar* is 4 km long

34.3 Mass Wasting Evolutionary Model

We discuss sequentially four evolutionary Stages of seamount subduction that produce distinct landsliding styles and abundance (Fig. 34.5). For each Stage we first describe the characteristic structures and then interpret the processes potentially controlling landsliding.

34.3.1 Stage 1: Seamount Collision with the Continental Margin Front

The initial collision of large seamounts is not currently occurring offshore Costa Rica, but the resulting structures can be studied from the morphology of deformational features at the base of the slope (Fig. 34.2).

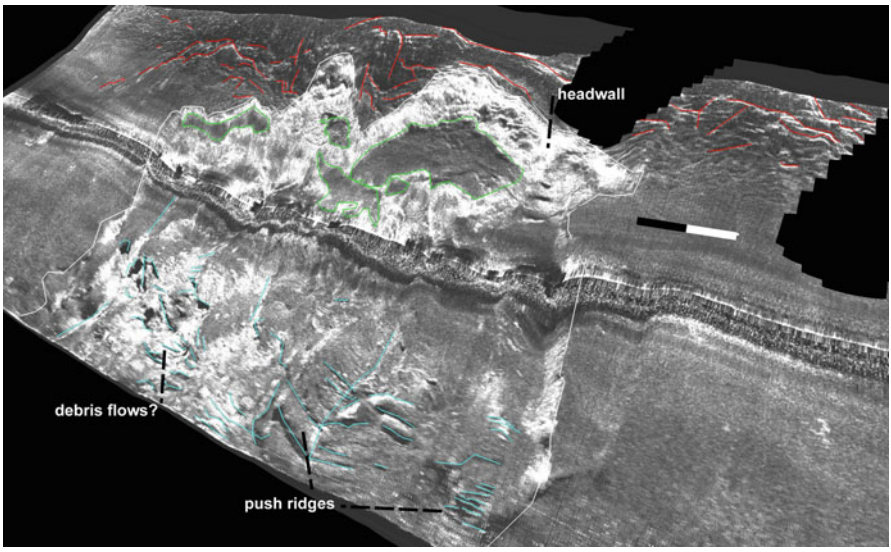

Fig. 34.4 Sidescan sonar imagery of Cabo Blanco translational slide complex. Sliding blocks and push ridges define Stage 4 processes. *Red lines* delineate main fractures of the swarm cutting slope sediment. *Pale blue lines* mark deformation structures in debris flows and push ridges. *Green polygons* delineate blocks. The *black-white bar* is 1 km long

The locus of recent collision are ~30–20 km wide by ~10 km deep landward indentations of the margin front clearly visible in multibeam bathymetry data (Fig. 34.1) that have been previously indentified (Ranero and von Huene 2000; von Huene et al. 2000, 2004). The smooth reentrant seafloor narrows inboard from ~20 km width where the entire frontal sediment prism has been removed, to ~5 km width. The transfer of upper plate material removed to form the indentations is unclear.

The fracture pattern of the lower slope changes from roughly trench parallel to strongly oblique near the reentrant (red fractures in Fig. 34.2) indicating that the seamount fractured and pushed sideways the margin basement and overlying sediment.

We interpret that during collision, before seamounts fully under-thrust the overriding plate, slope material is not uplifted above a seamount crest to fail in its wake, but is pushed in front and aside (Fig. 34.5a). Material pushed in front probably accumulates abutting the seamount flank and is under-thrust, which may involve at least part of the large mass of missing material in the reentrant (Fig. 34.2).

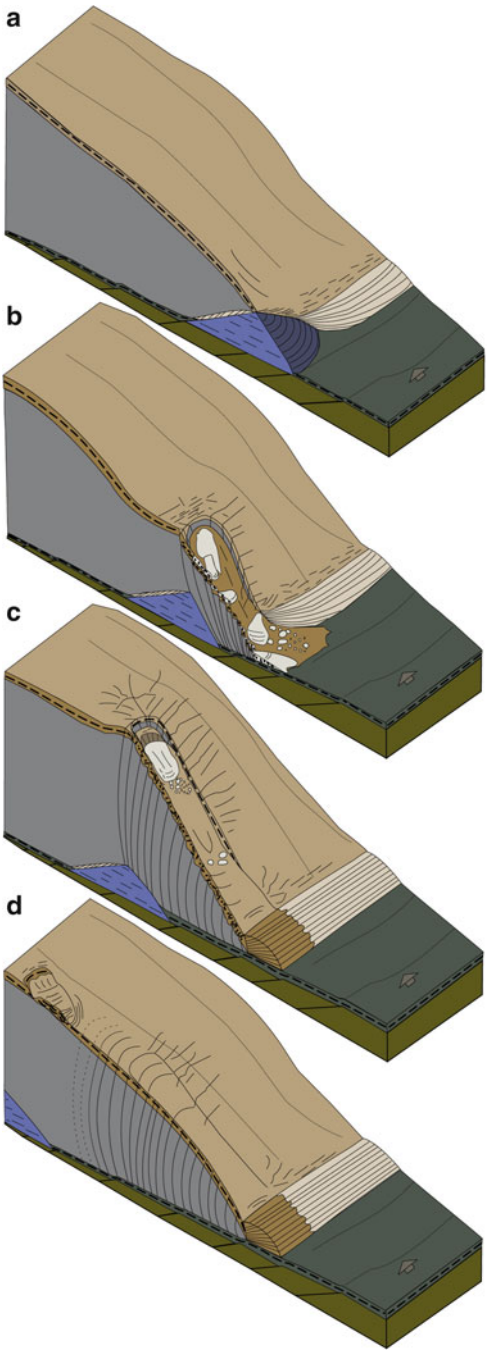

Fig. 34.5 Conceptual model of deformation and associated mass wasting processes related to seamount subduction. (**a**) Stage 1: Seamount collision with continental margin front. (**b**) Stage 2: Initial seamount thrusting under the *upper* plate and associated rock avalanches. (**c**) Stage 3: Seamount tunneling of overriding plate and associated rotational slumps. (**d**) Stage 4: *Upper* plate flexing and associated translational slides

34.3.2 Stage 2: Initial Seamount Thrusting Under the Continental Slope: Formation of Rock Avalanches

As a whole seamount under-thrusts the competent margin-wedge rock, upper-plate deformation and mass wasting processes change. The seamount uplifts the slope forming a fractured dome, and mass wasting occurs localized in the wake trailing the seamount (Fig. 34.1). Parrita shows an uplifted slope with a dome intensely cut, principally by trench-parallel fractures, ~1–5 km long, and a few hundreds of meters apart (Fig. 34.2). Radial fractures, described in analog models (Dominguez et al. 1998) are rare at Stage 2.

The terrain produced by failure forms trench-perpendicular depressions and intervening ridges that indicate the maximum width of failed rock masses (Fig. 34.2). The relief of the failed slope is characterized by sidewalls and headwalls up to 1 km high and 20–30° steep, that reach up to 35° in the uppermost sector.

We interpret that trench parallel fractures of the dome precondition the upper plate to fail in a complex mode. The steepest uppermost sector conforms a headwall that strikes parallel to fractures at the dome, which may indicate that it was formed by failure along a pre-existing fracture.

Types of mass-wasting deposits change from the foot to the top of the scar, possibly indicating an evolution in mass wasting processes. The smooth seafloor of the re-entrant from Stage 1 is covered close to the slope by a large (~4 × 6 km) debris flow containing coherent blocks generated during the first failures of Stage 2 (Fig. 34.2). Failed blocks littering the trench axis range from a few tens to several hundreds of meters. Blocks contained in the debris flow may be contemporary with that event. Others are away of the debris flow and possibly come from a different rock avalanche. Upslope along the scar, most of the seafloor is covered by overlapping debris flows, ranging from a few hundreds of meters to ~2 km in width and ~2–4 km long, that often appear to derive from the sidewalls and flanks of ridges (Fig. 34.2).

In the upper third of the scar, debris flows are rare. Here, sidescan sonar imagery is characterized by high backscatter, possibly indicating more recent mass wasting processes related to the disintegration of detached blocks that travel downhill, creating rock avalanches, that may turn into turbidities traversing down slope before reaching the trench axis. Turbidites fill the re-entrant produced in Stage 1 smoothing the seafloor between Parrita scarp and bending-related faults in the oceanic plate.

The deformation inferred from surface structures may involve fracturing of the entire overriding plate (Fig. 34.5b). Stage 2 occurs when a 2–4 km tall seamount is a ~1–4 km thick upper plate, as under Parrita (Ranero and von Huene 2000). We interpret that first the upper plate is uplifted and fractured possibly to a shallow depth where stresses are tensile. Fractures initially have small vertical offsets, but when the seamount subducts further, the fractures grow in its wake to 1 km offsets as the

entire upper plate collapses. Gravitational processes include sediment mass-wasting described above, and perhaps creep of fracture-bounded blocks involving the entire upper plate (Fig. 34.5b).

34.3.3 Stage 3: Seamount Tunneling of Overriding Plate: Formation of Rotational Slumps

As a large seamount travels deeper in the subduction zone, overriding plate deformation creates a trailing groove (Figs. 34.3 and 34.5c). The 3–4 km wide groove has sidewalls 25–30° steep that define fairly continuous faults. The sidewalls extend for >10 km from the edges of the headwall scarp, where they are ~1 km high, to diminish in height and disappear where sediment fills the groove (Fig. 34.3).

The uplift above the seamount forms a dome, with fracture spacing larger than in Stage 2. Fractures are ~1–5 km long, typically trench-parallel, but some are radial with morphology similar to analog models (Dominguez et al. 1998). The groove located trenchward of the dome, formed in the trailing wake of the subducting seamount, is narrower than fractures at the dome.

We interpret that groove formation involves upper-plate thinning and resulting subsidence through material removal by tectonic erosion by the subducting seamount (Ranero and von Huene 2000). The seamount dimensions and the elastic thickness of the upper plate probably control the constant width of the groove.

The length of the dome trench-parallel fractures does not control mass wasting during Stage 3. The dimensions of failing blocks appear preconditioned by the same characteristics that control the constant groove width. At Jaco, a $\sim 4 \times 1$ km block, abutting the headwall, has slid hundreds of meters (Fig. 34.3) indicating that, at least during a first phase, some blocks creep rather than catastrophically fail. The block seems cut by one oblique fracture into two sub-blocks that have slid slightly different amounts. The vertical dimension of the block is unclear and might be as thick as the entire headwall, so that the block is a coherent rotational slump that initially maintains its integrity. However, several debris flows located down-slope indicate that blocks may eventually disintegrate near the base of the headwall. In a similar process, a 1×0.5 km block has slid along the groove sidewall. The sidewalls foot is covered by comparatively smaller debris flows with tens-to-hundreds-of-meter-large blocks (Fig. 34.3).

We interpret that the surface deformation associated to Stage 3 occurring when a seamount is ~4–8 km deep under the seafloor involves deep faulting across the entire upper plate (Fig. 34.5c). The 1-km-high headwall and sidewalls dimensions mean deep penetrating faults. In addition to the slumps abutting the headwall, the entire upper plate is collapsing at depth along the flanks of the seamount as several-km-thick rotational blocks.

34.3.4 Stage 4: Upper Plate Flexing: Formation of Translational Slides

Above a large seamount that has subducted to a depth of 8–12 km the overriding plate flexes but fractures little, the deep grooves of Stage 3 no longer form and mass wasting processes become more sporadic and produce comparatively smaller scale structures (Fig. 34.4). The relief of the continental slope above the seamount displays comparatively little uplift and minor fracturing. The Cabo Blanco landslide complex shows a slope cut by a swarm of small, hundreds-of-meter-long fractures with an anastomosing pattern that form irregular slide headwalls, a few hundreds of meters high (Fig. 34.4).

At Stage 4, mass wasting appears dominated by translational sliding affecting the upper few hundreds meters of slope sediment. Sliding produces groups of detached blocks that have moved down-slope a few-hundreds-of-meters distance (Fig. 34.4). The characteristic push ridges at the front of the slid mass also support relatively short displacements, compared to slide events occurring during the other Stages.

We interpret that the processes active at Stage 4 are fundamentally different from those of previous Stages. The competent ~8–12 km thick overriding plate above the seamount does not break as in previous Stages (Fig. 34.5d). In addition to the attenuation through increased thickness of the upper plate, the material progressively eroded by seamount tunneling flows around the seamount and reduces the relief of the ocean plate. As a consequence, associated seafloor relief comparatively diminishes and minor uplift, related tilting and minor fracturing trigger shallow translational sliding probably using pre-existing weak layers, like ash layers that have been shown to precondition the slope sediment structure in the region (Harders et al. 2010). Thus, deformation and stresses related to seamount subduction, which precondition sediment landsliding for Stages 1–3, are not the only preconditioning factor at Stage 4.

34.4 Conclusions

Upper plate deformation resulting from subduction of tens-of-km wide and 2–3-km tall seamounts varies as seamounts traverse under an overriding plate. During Stage 1, seamounts breach the margin front, creating re-entrants by removing material, possibly by pushing some aside and also transporting some material abutting their frontal flank into the subduction zone. During Stage 2, seamounts first under-thrust the overriding plate, causing intense trench-parallel fracturing that preconditions complex mass-wasting processes. During Stage 3, seamounts move deeper, under a 4–8 km thick plate. Here, uplift creates trench-parallel and radial fractures. Material removal by seamount tunneling forms linear grooves with steep ~1 km

high headwalls and sidewalls that promote rotational slumps. These slumps creep some distance along the scarps to disintegrate down-slope into debris flows. During Stage 4 a seamount is under an 8–12-km-thick plate that is competent and deforms by minor fracturing and tilting. Here dominates translational sliding of shallow sediment, possibly using pre-existing weak planes. In summary, Stages 1–3 failures are preconditioned by deformation by seamount subduction, whereas Stage 4 failure appears preconditioned by a combination of deformation and pre-existing factors.

Acknowledgements Side scan sonar data were collected with the R/V Sonne using the TOBI system from National Oceanographic Center Southampton. We acknowledge the constructive reviews of R. von Huene and C. Lo Iacono.

References

Dominguez S, Lallemand SE, Malavieille J et al (1998) Upper plate deformation associated with seamount subduction. Tectonophysics 293:207–224

Harders R, Kutterolf S, Hensen C et al (2010) Tephra layers: a controlling factor on submarine translational sliding? Geochem Geophys Geosyst 11:Q05S23. doi:10.1029/2009GC002844

Harders R, Ranero W, Weinrebe CR et al (2011) Submarine slope failures along the convergent continental margin of the Middle America Trench. Geochem Geophys Geosyst 12:Q05S32. doi:10.1029/2010GC003401

Harders R, Ranero CR Weinrebe W et al (2012) An overview of the role of long-term tectonics and incoming plate structure on segmentation of submarine mass wasting phenomena along the Middle America Trench. Chapter 35 In: Yamada Y et al (eds) Submarine mass movements and their consequences. Advances in natural and technological hazards research, vol 31, Springer Science + Business Media B.V., Dordrecht. doi: 10.1007/978-94-007-2162-3_35

Hühnerbach V, Masson DG, Bohrmann G et al (2005) Deformation and submarine landsliding caused by seamount subduction beneath the Costa Rica continental margin—new insights from high-resolution sidescan sonar data. In: Hodgons DM, Flint SS (eds) Submarine slope systems: processes and products, Geological society special publication 244. The Geological Society, London, pp 195–205

Kluesner JW, Silver EA, Bangs NL et al (2013) High density of structurally-controlled, shallow to deep water fluid seep indicators imaged offshore Costa Rica. Geochem Geophys Geosyst 11:1525–2027. doi:10.1002/ggge.20058

Ranero CR, von Huene R (2000) Subduction erosion along the Middle America convergent margin. Nature 404:748–752

Ranero CR, Grevemeyer I, Sahling H et al (2008) The hydrogeological system of erosional convergent margins and its influence on tectonics and interplate seismogenesis. Geochem Geophys Geosyst 9:Q03S04. doi:10.1029/2007GC001679

von Huene R, Ranero CR, Weinrebe W et al (2000) Quaternary convergent margin tectonics of Costa Rica, segmentation of the Cocos Plate, and Central American volcanism. Tectonics 19:314–334

von Huene R, Ranero CR, Watts P et al (2004) Tsunamigenic slope failure along the Middle America Trench in two tectonic settings. Mar Geol 203:303–317

Werner R, Hoernle K, van den Bogaard P et al (1999) Drowned 14-m.y.-old Galápagos archipelago off the coast of Costa Rica: implications for tectonic and evolutionary models. Geology 27:499–502. doi:10.1130/0091-7613